Polyisobutylene and carbon nanotube based heterostructure SAW sensor for detection of TCM gas

Ashish Tiwary
Electronics and Communication Engineering
GIET University Gunupur
Rayagada, India
ashishtiwary@giet.edu

Subhrajit Pradhan
Electronics and Communication Engineering
GIET University Gunupur
Rayagada, India
subhrajitpradhan@giet.edu

Basudeba Behera
Electronics and Communication Engineering
National Institute of Technology
Jamshedpur, India
basudeb.ece@nitjsr.ac.in

Jitendra Kumar
Electronics and Communication Engineering
GIET University Gunupur
Rayagada, India
jitendrakumar@giet.edu

***Abstract*— The paper presents a study on surface acoustic wave (SAW) one-port resonating sensor device using 2-D modelling based on finite element method (FEM). The proposed SAW resonator structure was modeled with aluminum inter-digitated transducer (IDT) metallic electrodes over Lithium Niobate piezoelectric substrate. The SAW sensor model was designed with the carbon nanotube with a sensing polymer layer polyisobutylene, which helps in the detection of the various properties of the target gas i.e., Trichloromethane (TCM) at room temperature. The sensing characteristics was compared with other volatile organic compounds at 100 ppm of gas concentration. The eigen frequencies were measured either by exposure of target gas or without over the sensing layer. The model shows the significant shift in resonant frequencies (Δf) for 100 ppm gas concentrations. Sensor admittance (Y_{11}) parameter, change in CNT thickness and electric potential distribution for the TCM SAW sensor were investigated. The outcome of various response for multilayered SAW sensor shows better performance in terms of sensitivity, and found to be the most suitable for sensing TCM.**

Keywords— Finite element method, Lithium Niobate, carbon nanotube, polyisobutylene, Trichloromethane

I. INTRODUCTION

In the current scenario, human health becomes a major concern for the society which entirely depends on environmental conditions. It is quite a difficult task to strengthen a healthy life in such polluted atmosphere where the existence of toxic gaseous elements is growing day wise [1]. This leads to rapid emergence of lung ailments, skin infection and other threatening medical disorders like carcinoma, liver damage, hyperglycemia etc. A proper detection and observation of air quality is highly required, to get prevent from these diseases. With the advent of the technology, development of the sensors which can measure the toxic gases, is a huge challenge and importance for today's researcher. The category of carbon-based chemical compounds known as volatile organic compounds (VOCs) includes molecules that readily float in the air at normal climate [1]. These compounds are generally found in cosmetics, varnishes, personal care items, industrial operations, paints and waxes, among other things. Some examples of VOCs are dichloromethane, ethanol, benzene, toluene, methanol, dichloroethane, acetone, chlorofluorocarbons, and methylene chloride. Capacitive and resistive gas sensors, chemical, potentiometric, and surface acoustic wave sensors are only a few of the sensor types that have been created so far for the detection of VOCs [2].

SAW technology offers a robust framework to detect VOCs in gaseous and fluidic phases in an accurate manner [1]. Composite materials such as polymers and nanoparticles have considerably enhanced the sensitivity of the sensor used to construct the heterostructure design model. The nanofilms are constructed with highly sensitive elements such as graphene oxide [2], CNT, or ZnO nanorods. SAW sensor for various gases exhibit optimum sensitivity choice along with a rapid reaction time. With the advent of technology based on piezoelectric material, the SAW device has the capability to detect the size of contaminants available in the gas at a very minute scale [3]. Among all other gas sensors, enhancement of the SAW device sensitivity makes an optimum choice for the industry related work. The device sensitivity analysis can be carried out with the measurement of output frequency in terms of frequency shift, proportional to the mass of gaseous molecules absorbed by the sensitive material at the sensor surface [4]. The incorporation of nanotubes onto the sensing layer of piezoelectric substrate proven to be the most promising layer in the making of gas sensor [5]. Surface acoustic wave devices yields resonance frequency were affected with the change of IDT and chosen piezoelectric substrate dimension.

SAW sensor based on Rayleigh wave has shown high sensitivity because of a significant portion of energy is concentrated on the substrate surface [6]. A piezoelectric substrate, IDT, and sensing layer built up the three significant parts of SAW gas sensor [7]. The SAW gas sensor works by interacting with an acoustic wave that is traveling through the substrate with a sensing layer whose properties, such as density, stiffness, conductivity, and permittivity, modify with the absorption of gases [8]. Phase variation in received signal and frequency shift in an oscillator system are investigated to determine the analyte-induced changes in acoustic wave velocity propagating through the sensing layer. The polymer sensing layer and IDTs in SAW sensors are built on a piezoelectric substrate. A certain amount of voltage produced with the mechanical force applied directly onto the device. This results in the voltage variation which depends on size and direction of the applied force. The device piezoelectric substrate composition influences the acoustic wave's velocity, which ranges between 1500 and 4800 m/s [9].This work shows a design of SAW one-port resonator in MHz

frequency range incorporated with CNT, suitable for detection of TCM compared with other toxic gases available in the environment. In the proposed work, the response of the SAW one-port resonator has been examined and the result was compared with available TCM SAW sensor.

II. MODELLING OF SURFACE ACOUSTIC SENSOR

Modeling of a SAW one-port resonating sensor device is shown in Fig. 1. The IDTs are placed periodically on a piezoelectric substrate. A voltage source V_{in} with its internal resistance R_{in} is applied to the bus bars of input IDT which allows the current to flow inside the IDT fingers [10]. The IDT is made up of aluminum material that produces a vibration in the fingers and gives rise to acoustic (mechanical) waves. These acoustic waves propagate through the piezoelectric substrate and

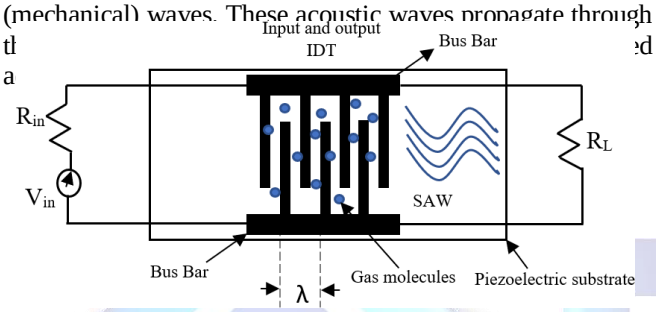

Fig. 1. Schematic of SAW one-port resonator device.

The incoming acoustic wave signals at the output IDT are converted into an electrical signal in the form of SAW output frequencies that would be calculated in terms of frequency shift. A calculated amount of target gas particles in parts per million (ppm) is allowed to reach at the sensing region of the piezoelectric substrate surface for the chosen model. Precisely, changes in acoustic wave velocity, mass loading, amplitude (successive peaks), and frequency shift can be observed. The potential distribution is computed in Fig. 2 for a 2-D issue i.e., *xy* plane by varying the voltage level. Here, in the inside specified region, potential distribution into squares of length '*h*' on a side is required.

The model parameters such as stress, strain, electric field, and electric displacement are represented by equation (1-2) [11]:

$$T = c_E S - e^T E \tag{1}$$

$$D = eS - \varepsilon_s E \tag{2}$$

where T is the stress matrix, S is the strain matrix, E [V/m] termed as the electric field, D termed as the electric displacement matrix [C/m^2], c_E termed as the elasticity matrix [Pa], e^T termed as the piezoelectric matrix [C/m^2] and ε_s termed as permittivity matrix. We have assumed in equation (3), the region to be charge free i.e., ∇. D = 0 or ∇. E = 0 and for a 2-D model;

$$\frac{\partial E_x}{\partial x} + \frac{\partial E_y}{\partial x} = 0 \tag{3}$$

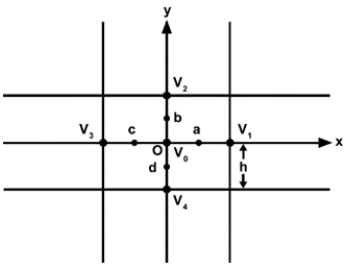

Fig. 2. Computational model of potential distribution.

Now the Laplace equation is given by the equation (4) as;

$$\frac{\partial^2 V}{\partial x^2} + \frac{\partial^2 V}{\partial y^2} = 0 \tag{4}$$

Approximate values for these partial derivatives can be obtained. The potential (V_0) at geometrical mid-point i.e., origin of the model is obtained from equation (5-9), where potentials at nearby symmetric points are known. Now, from the above figure 2;

$$\frac{\partial V}{\partial x}\Big|a = \frac{V_1 - V_0}{h} \tag{5}$$

$$\frac{\partial V}{\partial x}\Big|c = \frac{V_0 - V_3}{h} \tag{6}$$

From the gradients;

$$\frac{\partial^2 V}{\partial x^2}\Big|_0 = \frac{\frac{\partial V}{\partial x}\Big|_a - \frac{\partial V}{\partial x}\Big|_c}{h} \tag{7}$$

$$\frac{\frac{V_1 - V_0}{h} * - \frac{V_0 - V_3}{h}}{h} \tag{8}$$

$$= \frac{V_1 - V_0 - V_0 + V_3}{h^2} \tag{9}$$

Similarly,

$$\frac{\partial^2 V}{\partial x^2} + \frac{\partial^2 V}{\partial y^2} = \frac{V_1 + V_2 + V_3 + V_4 - 4V_0}{h^2} = 0 \tag{10}$$

$$V_0 = \frac{1}{4}(V_1 + V_2 + V_3 + V_4) \tag{11}$$

From the above equation (10-11), it is observed that the potential at mid-point 'o' is average of the potential at the four neighboring points.

A. *Proposed Design of SAW sensor*

In the proposed design of a SAW sensor, the impact of the influencing parameters has been studied using the SAW resonators, which have been designed and simulated. A metallic periodic structure in the form of a comb made up of aluminum material creates the wave in this instance by using the piezoelectric effect to transform electrical energy into mechanical energy further shown in Fig. 3. Here, each IDT finger width spacing is confined to ($\lambda/8 + \lambda/4 + \lambda/8$) the size of the unit cell ($\lambda = 4$ μm).

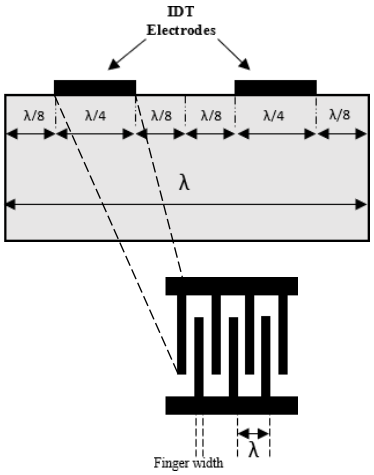

Fig. 3. A schematic of SAW resonator with alternating IDT electrodes.

Two neighboring IDT pairs are separated by the wavelength (λ/2). Two fingers and two spaces desribes a wavelength (λ) of the device. Each finger and space on an IDT are of the same width [12]. The wave velocity propagates throughout the substrate wavelength, can be used to compute the frequency of an acoustic wave since the polarity of the electrodes on two adjacent IDTs is opposite associated with the natural resonance eigenmode frequency. COMSOL Multiphysics simulation tool has been used to carry out FEM to explore the features of the generated SAW propagation velocity of 3488 m/s.

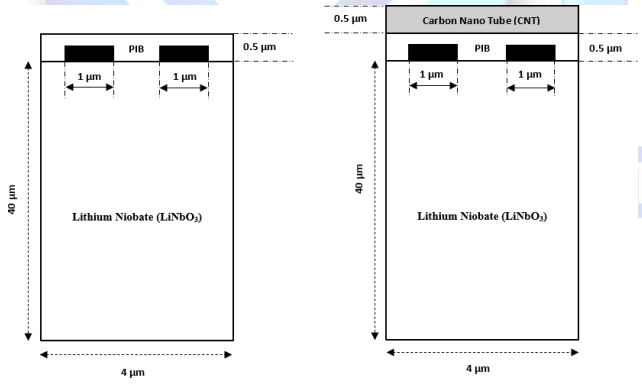

Fig. 4. Schematic of SAW device with sensing layer (a) PIB/$LiNbO_3$, (b) CNT/PIB/$LiNbO_3$.

A PIB polymer sensor was constructed in this work model at early phase to estimate resonance frequency (f_r), and the anti-resonance frequency (f_{ar}) which displayed an irregular shift in frequency. The several parameters necessary to create such sensors were computed based on these results and compared to multi-layered structures or heterostructures. Fig. 4 outlines a 2-D geometry derived from a three-dimensional model where monolayered and multi-layered structures have been depicted. A one-port SAW resonators consists of two IDT fingers, each having its own size. In this instance, the radio frequency (RF) signal is applied to the IDT electrodes, which produces a vibrational effect as a result of the opposite piezoelectric material functioning as an elastic body [13].

Certain acoustic waves are produced by this vibration and propagates along the piezoelectric substrate's surface. SAW signals can be developed and detected by periodic interdigitated electrodes on a piezoelectric plane surface. A Radio Frequency (RF) source is applied to the IDT terminals, a periodic electric field is created, enabling piezoelectric incorporate to a propagating surface wave plane [14]. In order to convert maximum electrical energy to mechanical, a RF signal is supplied to the IDT bus bars with the frequency (f). As a result, the relation between $'f'$ and periodicity 'λ' of SAW model is expressed in equation (12) as;

$$f = f_0 = \frac{v_s}{\lambda} \tag{12}$$

where v_s is the velocity of surface acoustic wave and f_0 is the center (operating) frequency of the SAW sensor. A major factor in selecting the center (operating) frequency while modelling the sensor structure is the velocity of SAW propagation. The surface wave electro-mechanical coupling co-efficient (k_s^2) is meant to be another significant feature for wide range of applications [15]. This element is characterized by the change in SAW velocity occurred, propagates along the piezoelectric surface enveloped with the weightless conductor. This is achieved essentially after short-circuiting the piezoelectric material.

The surface wave electro-mechanical coupling co-efficient (k_s^2) is measured by equation (13);

$$k_s^2 = 2(v_{free} - v_{met.})/v_{free} \tag{13}$$

where, v_{free} is the free surface wave velocity and $v_{met.}$ is the metallized surface velocity where IDT fingers are coated on the piezoelectric substrate.

As long as the gaseous ions are not in contact, the sensing layer is in thermal equilibrium. Once reached, the adsorption rate is accelerated by a significant concentration of gaseous chemical species deposits on the sensor layer [16]. This results in mass loading effect rises due to the adsorption phenomena occurred, and eventually a small variation in the SAW velocity led to a frequency shift that can be determined from the equation (14);

$$\Delta f = (k_1 + k_2) f_0^2 t K C \tag{14}$$

where, k_1 and k_2 termed as coupling constants, t is the thickness of the layer in µm, K termed as air/partition constant for various gases and C is the gas concentration in ppm.

In general, the measurement of gas sensor sensitivity (S) can be calculated as the ratio between the change in sensor response (ΔR) to the gas concentration (Δn), i.e., S =$\Delta R/\Delta n$. Therefore, the increase in the value ΔR concerning frequency shift compared to other sensors for the same mass loading

will definitely provide a higher sensitivity [17]. The relationship between ΔR, surface acoustic wave velocity and mass loading can be represented by the equation (15) as;

$$\Delta R = \frac{\Delta v}{v} = \frac{\Delta f}{f_0} = (k_1 + k_2) f_0^2 \Delta m / A \qquad (15)$$

where Δv is the change in wave velocity, v is the unperturbed velocity on the piezoelectric substrate, A is the surface area and Δm is the mass loading variation onto gaseous substance [18]. In this study, 128° YX-cut Lithium Niobate is used as the piezoelectric crystal substrate material. The acoustic wave velocity of Rayleigh wave is considered as ~3488 m/s with high electromechanical coupling coefficient, being more stable, and having lower wave transmission loss compare to other piezoelectric substrate materials [19]. The COMSOL Multiphysics simulation tool has been used to create and simulate multilayer 2-D structures. The SAW acoustic sensor enables IDTs constructed of aluminum metal electrode or gold during the simulation.

The rigidity of the piezoelectric surface layer is altered by TCM gas exposure and is now being assessed for the heterostructure design in equation (16-18) [20];

$$\rho_{TCM} = \text{KMC} \qquad (16)$$

$$C = (C_0 \times 10^{-6} \times P)/RT \qquad (17)$$

$$K = 10^{4.36} \qquad (18)$$

where, C_0 is the gas concentration in ppm, M is termed as molar mass, C termed as the gas concentration present in air, and K termed as an air/PIB partition coefficient for TCM, where ρ_{TCM} is termed as the TCM density, P is the pressure, T defined as temperature, R is universal gas constant.

III. RESULTS AND DISCUSSION

The foremost goal of this study is to investigate and compute responses from the proposed heterostructure device with the chosen specific piezoelectric substrate $LiNbO_3$ with and without the subjection of gas molecules. The simulated structure was compared for experimental verification with other VOCs. During the wave propagation, IDTs transform an electric signal into SAW frequencies using harmonics that are multiples of the fundamental frequencies [21].

In this work, the structures show a variation in certain parameters such as frequency shift and displacement with a change in the parameter value. The SAW gas sensors were built with mixture material such as PIB polymer and CNT as sensitive layers. This multi-layered device was studied for the measurement of change in frequency for the amount of TCM gas absorbed on the sensing layer. A PIB layer was placed on the $LiNbO_3$ substrate without CNT material, made up the first structured model. In Fig. 5, the sensor model was tested with the exposure of TCM gas on PIB layer without CNT coating, results in no change in frequency in a one-port SAW resonator.

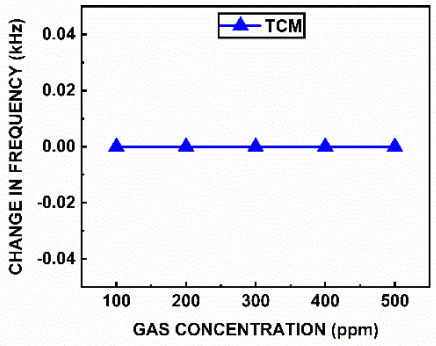

Fig. 5. Plot between change in frequency and gas concentration without CNT coating.

With the coating of carbon nano materials on the PIB layer, the increase in mass loading has been observed as TCM absorption is high on the sensing layer shown in Fig. 6.

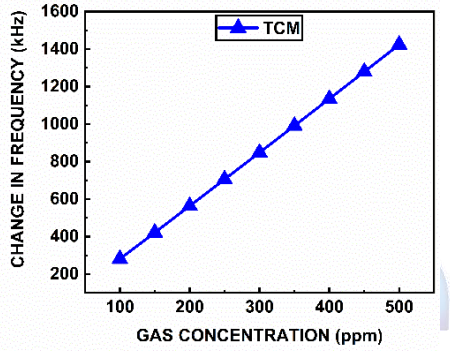

Fig. 6. Plot between gas concentration and change in frequency with CNT.

Our proposed model has been evaluated to understand the device outcome as for the change in the resonating signal frequency. This variation is observed with the change in CNT layer thickness ranges from lowest 0.3 µm to highest 1 µm. From Fig. 7, maximum Δf of 280.7 kHz is obtained in between 0.4 µm to 0.6 µm of CNT thickness for TCM gas. It was observed that with the change in CNT thickness, the sensitivity ($\Delta f/f$) is the same as the Δf.

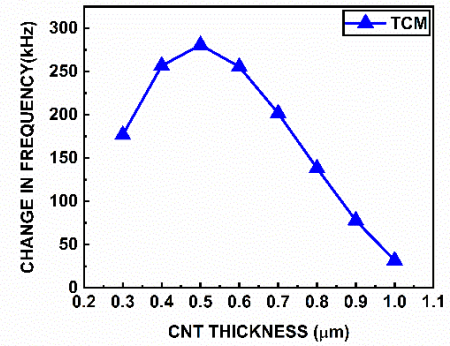

Fig. 7. Plot between Change in Frequency and CNT Thickness.

A. Simulation Results

The details of SAW device mentioned in the above Table I, the proposed sensor has been designed and simulated. A sub-micron layer of PIB having a depth of 0.5 µm has been layered on a piezoelectric substrate. The width and height of the substrate should be always in the 1:10 ratio to overcome the mechanical deformation of resonance and anti-resonance

effect [22]. Here, the piezoelectric substrate made up of $LiNbO_3$ material has a width dimension of 4 µm and a substrate height of 40 µm in the XZ plane system. The proposed sensor design added a second layer of CNT placed over PIB as a top layer to increase sensitivity and serve as an outstanding TCM adsorbent with a thickness of 0.5 µm. A comb-like structure, an IDT electrode of aluminium material is being chosen for the conversion of RF signal to the acousto-mechanical wave. The IDT of finger count two is now mounted on the $LiNbO_3$ substrate with a depth of 0.2 µm and the space between the fingers of 1 µm.

TABLE I SAW SENSOR PARAMETERS

Parameters	CNT/PIB/$LiNbO_3$
Gas Concentration	100 ppm
IDT depth	0.2 µm
Space between two IDT electrodes	1 µm
IDT thickness	1 µm
CNT depth	0.5 µm
PIB depth	0.5 µm
$LiNbO_3$ substrate width	4 µm
$LiNbO_3$ substrate height	40 µm
SAW resonating frequency	857.21 MHz
Free Surface wave velocity	3428.84 m/s

B. Multi-Layer structure (PIB/CNT/$LiNbO_3$)

The multi-layered structure exhibits a f_{ar} of 873.67 MHz and f_r effect of 857.21 MHz that has a transition from switch = 0 to switch = 1 shown in Fig. (8-11). The simulation result is obtained with and without exposure to TCM gas concentration on the sensing layer [23]. Due to this switching phenomenon, the quantity of the change in eigen frequency with respect to Δf and the displacement is computed for the heterostructure device SAW sensor.

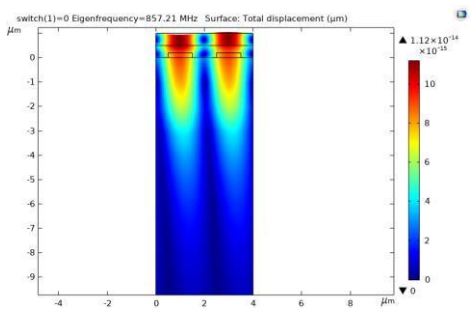

Fig. 8. Resonance effect of 857.21 MHz for the CNT/PIB/$LiNbO_3$.

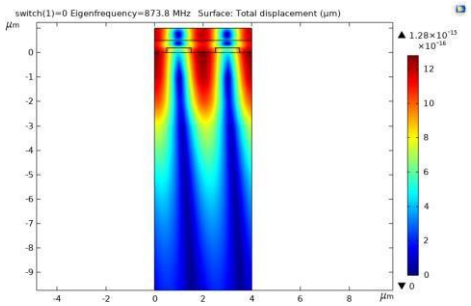

Fig. 9. Anti-resonance effect of 873.8 MHz for the CNT/PIB/$LiNbO_3$.

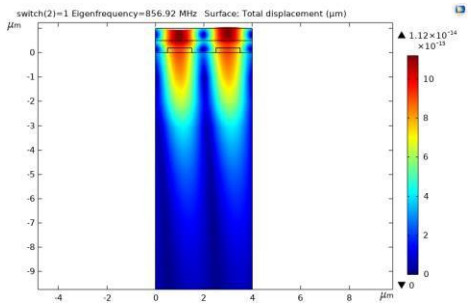

Fig. 10. Resonance effect of 856.92 MHz for the CNT/PIB/$LiNbO_3$ SAW sensor.

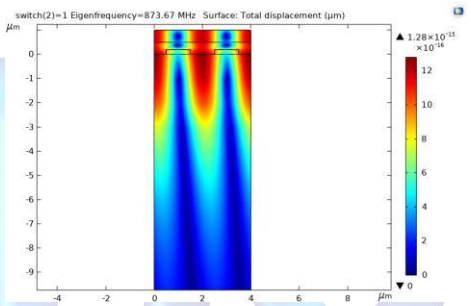

Fig. 11. Anti-resonance effect of 873.67 MHz for the CNT/PIB/$LiNbO_3$ SAW sensor.

From the Fig. (12-15), the surface potential distribution of heterostructure model for the SAW resonator has been simulated using the switching mode from 0 to 1 at both resonance and anti-resonance frequency.

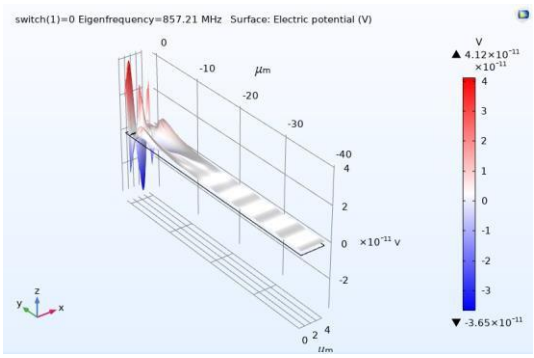

Fig. 12. Electric potential distribution (switch=0) at Resonance frequency.

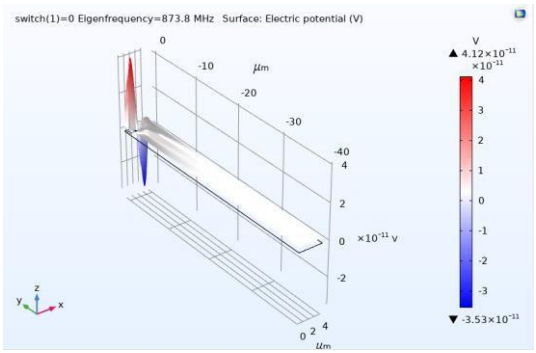

Fig. 13. Electric potential distribution (switch=0) at anti-resonance frequency.

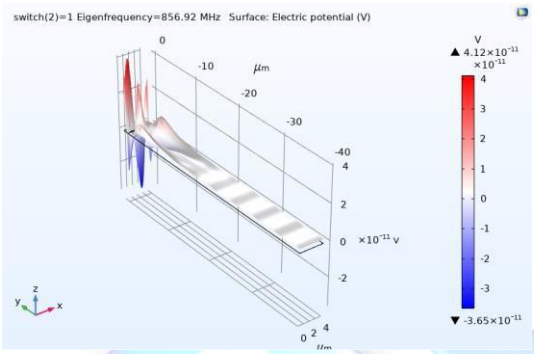

Fig. 14. Electric potential distribution (switch=1) at resonance frequency.

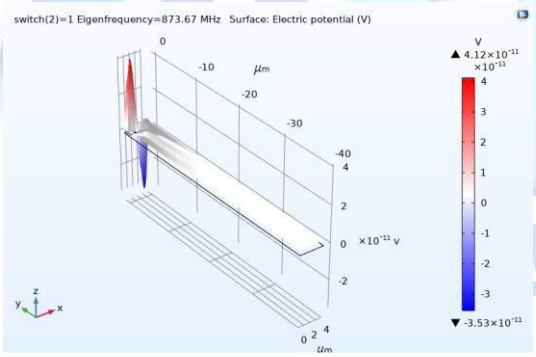

Fig. 15. Electric potential distribution (switch=1) at anti-resonance frequency.

The one-port SAW resonator performance is characterized by its absolute and imaginary admittances, shown in Fig. 16 below;

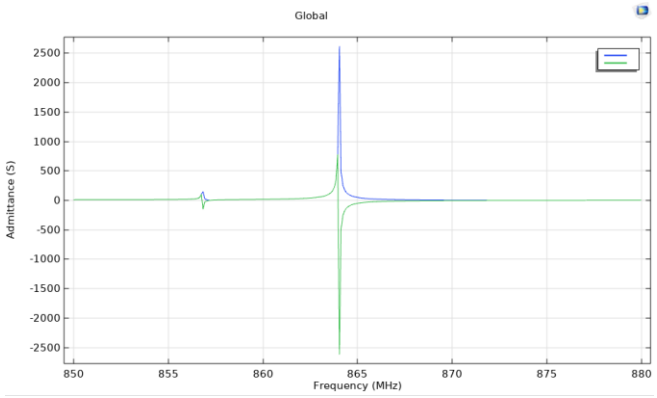

Fig. 16. The real and imaginary admittance of SAW sensor in frequency domain.

The simulated evaluation for TCM for 100 ppm gas concentration results in Eigen frequencies that define f_r and f_{ar} for the proposed SAW sensor. The IDTs electrode computes a specific lowest range of frequency shift (kHz), with or without the subjection of TCM gas on the sensor layer.

TABLE II COMPARISON OF FREQUENCY SHIFT FOR TCM GAS

Concentration of target gas (ppm)	Δf (kHz)	References
100	280.7	This work
100	1.394	[24]
100	1.840	[25]

The SAW heterostructure model (PIB/CNT/$LiNbO_3$) frequency shift (Δf) responses were compared with other research work in given Table II. These literatures used Lamb wave resonator on SOI/AlN substrate and Sezawa mode for TCM gas sensor with PIB layer respectively [24], [25]. The Δf for the same TCM gas at 100 ppm was studied. Our proposed one-port CNT/PIB/$LiNbO_3$ SAW TCM gas sensor shows Δf of 280.7 kHz whereas, 1.394 kHz and 1.840 kHz is observed in the previous research work done [24], [25].

Sensitivity of 3 kHz/ppm was reported for bulk acoustic wave (BAW) device at 1.377 GHz [26]. For similar device resonating frequency with the specified dimensions i.e., IDT width of 0.7 µm, λ of 2.8 µm with f_r of 1.245 GHz, we have achieved 3.18 kHz/ppm which is in comparison or even slightly better than the BAW devices [26].

High sensitivity of the proposed device is observed due to presence of CNT/PIB multilayer. The multi-layered CNT/PIB/$LiNbO_3$ SAW gas sensor for TCM detection shows the best results concerning frequency shift.

IV. CONCLUSIONS

In this work, SAW one-port resonating sensor device for TCM gas sensing has been modeled and the sensor performance was simulated by considering two different sensor design with and without PIB layer. The SAW resonating device were modeled in Finite Element Method based on COMSOL Multiphysics. The characteristics of the sensor were studied with change in the gas concentration and CNT thickness, at room temperature. When exposed to the target gas, the proposed multi-layered SAW sensor (PIB/CNT/$LiNbO_3$) provides a frequency shift of 280.7 kHz. It was observed that the resonant and anti-resonant frequencies changes as a result of modification in the sensor parameters. The SAW heterostructure provides an excellent outcome shows with an optimum sensitivity, Δf , and electrostatic potential distribution. These investigations can be further carried out for different volatile organic gases with suitable choice of sensing material and may lead to fabrication of the device for real time industrial applications.

REFERENCES

[1] Devkota, J., Ohodnicki, P., & Greve, D. (2017). SAW Sensors for Chemical Vapors and Gases. Sensors, 17(4), 801. doi:10.3390/s17040801.

[2] Balashov, S. M., Balachova, O. V., Braga, A. V. U., Bazetto, M. C. Q., Pavani Filho, A., and Moshkalev, S. (2013). "Kinetic Characteristics of the SAW Humidity Sensor Partially Coated with Graphene Oxide Thin Film," inSBMicro 2013: 28th Symp. Microelectr. Technol. Devices, 2013. Curitiba, Brazil, September 2–6, 2013 (Curitiba, Brazil: IEEE). doi:10.1109/sbmicro.2013.6676163.

[3] Xuan, W., He, X., Chen, J., Wang, W., Wang, X., Xu, Y., et al. (2015). High Sensitivity Flexible Lamb-Wave Humidity Sensor with Graphene Oxide Sensing Layer. Nanoscale 7, 7430–7436. doi:10.1039/c5nr00040h.

[4] Sivaramakrishnan, S., Rajamani, R., Smith, C. S., McGee, K. A., Mann, K. R., and Yamashita, N. (2008). Carbon Nanotube-Coated Surface Acoustic Wave Sensor for Carbon Dioxide Sensing. Sens. Actuators B: Chem. 132, 296–304. doi:10.1016/j.snb.2008.01.041.

[5] M. Penza, P. Aversa, G. Cassano, W. Wlodarski, K. Kalantar-zadeh, "Layered SAW gas sensor with single-walled carbon nanotube-based nanocomposite coating," Sens. Actuators B, vol. 127(1), pp. 168-178, 2007.

[6] A. K. Nagmani and B. Behera, "A Review on High Temperature Piezoelectric Crystal $La_3Ga_5SiO_{14}$ for Sensor Applications," in IEEE Transactions on Ultrasonics, Ferroelectrics, and Frequency Control, vol. 69, no. 3, pp. 918-931, March 2022, doi: 10.1109/TUFFC.2022.3143666.

[7] Jakubik WP (2011) Surface acoustic wave-based gas sensors. Thin Solid Films 520(3):986–993. https://doi.org/10.1016/j.tsf.2011.04.174.

[8] Tiwary, A., Rout, S.S. & Behera, B. Design and Analysis of Various Characteristics of a MEMS-Based PIB/CNT/$LiNbO_3$ Multilayered SAW Sensor for CO_2 Gas Detection. Trans. Electr. Electron. Mater. 23, 609–617 (2022). https://doi.org/10.1007/s42341-022-00392-x

[9] Hasan MN, Maity S, Sarkar A, Bhunia CT, Acharjee D, Joseph AM (2017) Simulation and fabrication of SAW-based gas sensor with modified surface state of active layer and electrode orientation for enhanced H2 gas sensing. J Electron Mater 46(2):679–686. https://doi.org/10.1007/s11664-016-5128-7.

[10] Behera, B., & Nemade, H. B. (2018). Investigating translational motion of a dual friction-drive surface acoustic wave motor through modeling and finite element simulation. SIMULATION, 003754971877877. doi:10.1177/0037549718778770

[11] Krishnasamy, Vinotha & Senthil Kumar, Vellingiri & Muruganand, Shanmugam & Manikandan, Nagarajan. (2018). Design and Simulation of Surface Acoustic Wave Sensor for Toxic Gas Detection. Journal of Advanced Research in Dynamical and Control Systems. 10. 491-500.

[12] Wang, L., & Wang, H. (2020). Analysis of propagation characteristics of AlN/diamond/Si layered SAW resonator. Microsystem Technologies. doi:10.1007/s00542-019-04658-y.

[13] Syamsu, I., Granz, T., Scholz, G., Mariana, S., Yulianto, N., Daul, L., … Wasisto, H. S. (2019). Design and fabrication of AlN-on-Si chirped surface acoustic wave resonators for label-free cell detection. Journal of Physics: Conference Series, 1319, 012011. doi:10.1088/1742-6596/1319/1/012011.

[14] Behera, B. (2019). Design and Investigation of a Dual-friction Drive based $LiNbO_3$ Piezoelectric Actuator Employing a Cylindrical Shaft as Slider. IEEE Sensors Journal, 1–1. doi:10.1109/jsen.2019.2938246

[15] Vanotti, M., Poisson, S., Soumann, V., Quesneau, V., Brandès, S., Desbois, N., Blondeau-Patissier, V. (2021). Influence of interfering gases on a carbon monoxide differential sensor based on SAW devices functionalized with cobalt and copper corroles. Sensors and Actuators B: Chemical, 332, 129507. doi:10.1016/j.snb.2021.129507.

[16] Behera, B. (2021). Micro motion of a piezoelectric linear actuator driven by liquid interacting with Rayleigh surface acoustic wave. Sensors and Actuators A: Physical, 331, 112756. doi:10.1016/j.sna.2021.112756

[17] Kumar, J., Nemade, H. B., & Giri, P. K. (2018). Adsorption of Small Molecules on Niobium Doped Graphene: A Study Based on Density Functional Theory. IEEE Electron Device Letters, 39(2), 296–299. doi:10.1109/led.2017.2787203

[18] Shen, J., Fu, S., Su, R., Xu, H., Lu, Z., Xu, Z., … Pan, F. (2021). High-Performance Surface Acoustic Wave Devices Using $LiNbO_3/SiO_2/SiC$ Multilayered Substrates. IEEE Transactions on Microwave Theory and Techniques, 69(8), 3693–3705. doi:10.1109/tmtt.2021.3077261.

[19] Su, F., Lu, C., & Hu, S. (2010). Adsorption of benzene, toluene, ethylbenzene and p-xylene by NaOCl-oxidized carbon nanotubes. Colloids and Surfaces A: Physicochemical and Engineering Aspects, 353(1), 83–91. doi:10.1016/j.colsurfa.2009.10.025.

[20] Abraham, N., Reshma Krishnakumar, R., Unni, C., & Philip, D. (2018). Simulation studies on the responses of ZnO-CuO/CNT nanocomposite based SAW sensor to various volatile organic chemicals. Journal of Science: Advanced Materials and Devices. doi:10.1016/j.jsamd.2018.12.006.

[21] Durani, F., Mainuddin, Mittal, U., Kumar, J., & Nimal, A. T. (2020). Use of Surface Acoustic Wave (SAW) for Thermal Conductivity Sensing of Gases – a Review. IETE Technical Review, 1–11. doi:10.1080/02564602.2020.1819888.

[22] Aslam, M., Jeoti, V., Karuppanan, S., Malik, A., & Iqbal, A. (2018). FEM Analysis of Sezawa Mode SAW Sensor for VOC Based on CMOS Compatible AlN/SiO_2/Si Multilayer Structure. Sensors, 18(6), 1687. doi:10.3390/s18061687.

[23] Zhang, C., Ghosh, A., Zhang, H., & Shi, S. (2019). Langasite-based surface acoustic wave resonator for acetone vapor sensing. Smart Materials and Structures. doi:10.1088/1361-665x/ab4739.

[24] Caliendo, C., & Hamidullah, M. (2017). Zero-group-velocity acoustic waveguides for high-frequency resonators. Journal of Physics D: Applied Physics, 50(47), 474002. doi:10.1088/1361-6463/aa900f.

[25] Laidoudi, F., Boubenider, F., Caliendo, C., & Hamidullah, M. (2019). Numerical Investigation of Rayleigh, Sezawa and Love Modes in C-Axis Tilted ZnO/Si for Gas and Liquid Multimode Sensor. Journal of Mechanics, 1–12. doi:10.1017/jmech.2019.14.

[26] Johar, A. K., Patel, R., Periasamy, C., Agarwal, A., & Boolchandani, D. (2018). FEM modeling and Simulation of SMFBAR sensor with PIB as Sensing layer for Tetrachloroethane (PCE) gas detection. Materials Research Express. doi:10.1088/2053-1591/aae73a